ORIGINAL ARTICLE

Adsorption studies on the removal of malachite green by γ-Fe$_2$O$_3$/ MWCNTs/Cellulose as an eco-friendly nanoadsorbent

Mansooreh khalatbary[1] · Mohammad Hossein Sayadi[1] · Mahmoud Hajiani[1] · Mohsen Nowrouzi[2]

Abstract

A highly efficient eco-friendly nanoadsorbent i.e. γ-Fe$_2$O$_3$/MWCNTs/Cellulose was derived from waste tires and natural cellulose for malachite green removal from aqueous solutions through a chemical vapor deposition technique. The properties of the synthesized nanoadsorbent were identified using XRD, FESEM, EDX, TEM, EDS, DLS, FTIR, VSM, BET, XPS, and TGA. According to the results, the highest malachite green adsorption capacity was obtained by γ-Fe$_2$O$_3$/MWCNTs/ cellulose 47.61 mg/g. In addition, the amount of dye adsorption increased with decreasing flow rate and enhancing column length from 9 to 3 mL/min and 2 to 10 min, respectively. The pseudo-second-order and the Langmuir model were the best kinetic and isothermal models to describe the malachite green adsorption process ($R^2 > 99\%$). The thermodynamic results demonstrated that the adsorption process is exothermic and spontaneous. However, after 4 consecutive adsorption/desorption cycles, the removal efficiency was 87.35%. Therefore, γ-Fe$_2$O$_3$/MWCNTs/Cellulose can be considered as an outstanding adsorbent for malachite green removal.

1 Introduction

Dyes are widely used in textiles, cosmetics, metal plating, and the pharmaceutical industry, and large amounts of dyed wastewater are produced and discharged in aqueous media. The discharge of effluents containing pigments into aquatic ecosystems not only damages beautiful natural landscapes but also prevents light from penetrating deep into the water and disrupts the process of photosynthesis, resulting in the destruction of aquatic ecosystems[1]. Dyes are considered a major environmental challenge due to their toxic, non-biodegradable, and potentially carcinogenic nature[2]. Malachite green (MG) dye with the chemical formula (C$_{52}$H$_{54}$N$_4$O) is a water-soluble cationic dye that belongs to the triphenylmethane group [3]. The presence of this dye in the food chain leads to carcinogenic effects and defects and chromosomal abnormalities in the fetus in humans. This dye readily decomposes and produces toxic by-products that lead to damage to the kidneys, liver, lungs, and bones [4, 5]. Hence, it is very vital to remove these dyes from the water bodies. Researchers have focused to remove these dyes from water and wastewater. So far, various methods such as electrochemical methods, biological methods, adsorption technology, coagulation and flocculation, and photocatalytic processes have been used to remove dye compounds [6, 7]. Degradation processes are a technique for the removal of organic pollutants such as dye into environmental solutions [8]. However, only able to slowly and partially mineralize these compounds, and many toxic by-products may remain in the environment. Although some of these advanced techniques are approximately expensive, but adsorption is a simple, cost-effective, and efficient technique for the adsorption of contaminants[9]. Adsorption method has been used as an efficient and effective method compared to other methods due to its cheapness, ease of performance control, non-toxicity, lack of sludge formation, and recoverability [10]. In this regard, a birds-eye view to utilize the biopolymers

✉ Mohammad Hossein Sayadi
  mh_sayadi@birjand.ac.ir

1 Department of Environmental Engineering, Faculty of Natural Resources and Environment, University of Birjand, Birjand, Iran

2 Department of Science and Biotechnology, Faculty of Nano and Bio Science and Technology, Persian Gulf University, 75169-13798 Bushehr, Iran

as a source for nanomaterials synthesis illustrates that cellulose is the most abundant biodegradable polymer derived from renewable polysaccharide resources for this purpose. Also, cellulose is one of the most plentiful biomaterials on the earth, which is produced in about 1011 tons per year [11]. Cellulose has three hydroxyl groups (OH^-) in each unit of hydroglucose and due to its very effective functional groups; it has an excellent performance in absorbing and removing environmental contaminants such as metal ions, inorganic anionic contaminants, heavy metals, and emerging pollutants and dyes [12–14]. Unlike these advantages, the low adsorption capacity of cellulose is the main restriction for its large-scale application but this deficiency can be remarkably improved just by a slight modification [15]. However, dealing with the applied carbon-based materials for the synthesis of highly efficient adsorbents, carbon nanotubes (CNTs) are among the most well-known ones in various industrial applications including gas sensors, capacitors, batteries, and biosensors because of their special physical and chemical properties, structural control, low density, and porosity [16–18]. Regarding this, many studies have introduced CNT as a very suitable and promising adsorbent for the rapid removal of contaminants from water and wastewater [19], and also to improve the mechanical, thermal, and electrical properties of Cellulose [20]. CNTs can be strongly bound to cellulose due to non-covalent interactions [21], resulting in the improvement of tensile strength of cellulosic materials and the enhancement of its removal potential of contaminants [19].

In the present study to augment the conformity and the adaptability of synthesized nanoadsorbents with the environmental criteria, the applied Multi-Walled Carbon Nanotubes(MWCNTs) was creatively manufactured by waste tires utilization through the chemical vapor deposition (CVD) method. Due to the increasing demand for automobiles worldwide, the environmental problems caused by the disposal of waste tires have become more serious because these materials are not biodegradable. Waste tires are extremely wealthy with carbon element content (88%), different elastomers (e.g. natural rubber, butadiene, and styrene-butadiene rubber), and metal reinforcements (such as sulfur, zinc, carbon strengthener/filler) [22]. Therefore, the reuse of waste tires can play a key role in the reduction of hazardous components release and their associated concerns. Addressing literature [23], the pyrolysis of waste tires is a good way to recover up to 90% of the residual content of carbon at high temperatures. However, despite all profits, the separation and recycling of CNT/Cellulose catalysts is a noticeable challenge for their application in water and wastewater treatment. To overcome this problem, the use of magnetic nanoparticle-based adsorbents has been recently paid great attention to because of their special properties such as small size and easy separation through

external magnetic fields [24]. In light of this fact, maghemite (γ-Fe_2O_3) is one of the most attractive iron oxides because of its chemical stability, biological compatibility, and heating ability which has been used in different applications such as pigments removal, photocatalytic analyses, and ferrofluid technology [25]. Therefore, the main objective of this study was the synthesis of a high efficient nanoadrorbent for significant removal of MG from aqueous solutions with the highest economic and environmental compatibility to provide a guideline for further investigations.

2 Materials and methods

2.1 Materials

Iron (II) Chloride Tetrahydrate ($FeCl_2.4H_2O$), Hexamethylenetetramine ($(CH_2)_6N_4$), Sodium Hydroxide (NaOH), Sodium Nitrate ($NaNO_3$), Epichlorohydrin (C_3D_5ClO), Urea, Ammonia, Sulfocarbamide, Dimethyl Formid ($(CH_3)_2NCH$), and malachite green dye with the chemical formula ($C_{52}H_{54}N_4O_{12}$) were purchased from Sigma Aldrich, USA. Commercial cellulose materials, containing 93% cellulose, were purchased by Pasargad Scientific Industrial Manufacturing Company (KANGAROO) and used without further purification. The waste tire specimen used in this study were Bridgestone disposable tires. Ferrocene, which was used as a source of Fe catalyst, was purchased from Sigma-Aldrich, USA. Due to the chemical structure of Fe ($C_5H_5)_2$, ferrocene has a dual function (it can act as a catalyst and carbon source) and therefore is effective in the production of CNT. During the research, deionized water was used to prepare the solutions.

2.2 Preparation of γ-Fe₂O₃ nanoparticles

To prepare γ-Fe_2O_3 nanoparticles, 21 g of iron (II) chloride tetrahydrate ($FeCl_2.4H_2O$), 25 g of hexamethylenetetramine ($(CH_2)_6N_4$), and 6 g of sodium nitrate ($NaNO_3$) were dissolved in 500 ml of distilled water. To prepare γ-Fe_2O_3 nanoparticles, 21 g of iron (II) chloride tetrahydrate($FeCl_2.4H_2O$), 25 g of hexamethylenetetramine ($(CH_2)_6N_4$) and 6 g of sodium nitrate ($NaNO_3$) were dissolved in 500 ml of distilled water. Then, these materials were mixed to attain a black precipitate. The precipitate was a permanent oxygen pump for 7 h at 60 °C before it was filtered by filter paper. The residue on the filter paper was washed several times with ethanol and distilled water to eliminate organic impurities and anions and then dried for 48 h at 55 °C. Finally, the dried specimens were ground and γ-Fe_2O_3 magnetic nanopowder was obtained[26].

2.3 Preparation of environmentally friendly carbon nanotubes

In this study, an environmentally friendly method was used to synthesize carbon nanotubes. The waste tire specimen used in this study was Bridgestone disposable tires. In this study, Ferrocene is used as a source of Fe catalyst because of the chemical structure of $Fe(C_5H_5)_2$. Ferrocene vaporized at a temperature above 400 °C. For this purpose, the waste tires were prepared and cut into tiny pieces and placed in a container and put in a furnace at 350 °C for 15 min in an inert nitrogen atmosphere with a flow rate of 3 L/min. The residue was manually crushed in a mortar and the resulting fine powder was used as carbon pre-production to synthesize carbon nanotubes. 2 g of the remnant fine powder was blended with 50 mg of ferrocene (as a catalyst) in a plant container and placed in a horizontal quartz tube, and then the system was drained under a nitrogen stream for 1 h. This process was started at ambient temperature and continuously enhanced at a rate of 30 °C/min, and it received the combustion temperature at 800 °C and placed on at this temperature for 30 min, then the chamber was turned off and allowed to cool down to the ambient temperature. At last, the tubes were opened and the resulting solids were collected. It should be noted that the synthesis of carbon nanotubes was used by chemical vapor deposition (CVD) due to its high performance and relatively low cost depending on the decomposition of hydrocarbons on the surface of catalysts of transition metals [27].

In the next step of preparing carbon nanotubes, the purification technique was carefully adjusted to reduce the damage in the structure of the synthesized MWCNTs. Since the MWCNTs prepared by CVD techniques were attendant with different types of carbon particles, it was crucial to apply a strong oxidant to purify the raw MWCNTs. Thus, at this stage, the as-synthesized MWCNTs were refined with a blend of concentrated H_2SO_4 and HNO_3 in a volume ratio of 3: 1. The amount of acid used was determined by the stoichiometry of the reaction between these acids and iron. The crude MWCNTs nanoparticles were dissolved in a mixture of these acids and vigorously stirred at ambient temperature for 48 h. Then, they washed several times with distilled water until the pH reached about 7. Then, the nanoparticles were dried at 120 °C for 12 h.

2.4 Preparation of magnetic nanoparticles MWCNTs

To synthesize MWCNTs magnetic nanoparticles, the first, 20 g of $FeCl_2.4H_2O$, 26 g of $(CH_2)_6N_4$, and 6 g of $NaNO_3$ were dissolved into 500 ml of distilled water. Then, 0.2 g of MWCNTs were added to them and the mixture was stirred for 2 h, and then the suspended was transferred into sonicated. In the next step, a solution of ammonia and water was added drop-wise into the mixed solution into sonicate. After the suspension was stable for 48 h, the products were separated and collected using an external magnet, and then washed several times with deionized water and ethanol. Finally, the resulting precipitate was dried in the oven at 80 °C for 7 h [28].

2.5 Magnetic γ-Fe$_2$O$_3$/MWCNTs functionalized cellulose

In order to functionalize nanoparticles, the preparation process is as follows: 6 wt% aqueous NaOH solution, 5.5 wt% sulfocarbamide, and 8.8 wt% urea are blended and the suspension was pre-cooled in a refrigerated at -4 °C[29]. 3 g of crude cellulose were immediately dissolved in 100 ml of aqueous solution at 25 °C for 5 min to give a clear cellulose solution by 3 wt% concentration. Sulfocarbamide, NaOH, and urea in a suspension can form hydrates that can react with cellulose, thereby dissolving cellulose and forming a clear cellulose solution[30]. In the next step, the cellulose solution was centrifuged at room temperature for 15 min at 8000 rpm to remove insoluble components and air bubbles. Then, 1 g of γ-Fe$_2$O$_3$ nanoparticles and 0.27 g of MWCNTs were added into the cellulose solution under a magnetic stirrer for 1 h. The resulting solution was poured into a coagulation bath containing 10 wt% sodium chloride and stirred. Once the soluble cellulose is coagulated again, γ-Fe$_2$O$_3$ and MWCNT were trapped by strip cellulose. After 12 h, 3 ml of epichlorohydrin was added drop-wise into the mixture by stirring for 50 min. Then, the mixture was increased to 80 °C by stirring for another 120 min to achieve γ-Fe$_2$O$_3$/MWCNTs/cellulose [31]. Finally, the resulting nanoparticles were separated using an external magnet and washed with ethanol and distilled water, and then dried in the oven at 70 °C for 8 h.

The stepwise preparation of γ-Fe$_2$O$_3$/MWCNTs/Cellulose is schematically depicted in Fig. 1. As can be seen, the synthesis of this nanoadsorbent was carried out at five distinct stages as follows: 1) MCNTs synthesized from waste tire, 2) MCNTs purification, 3) γ-Fe$_2$O$_3$ preparation, 4) γ-Fe$_2$O$_3$/MWCNTs synthesis, and 5) γ-Fe$_2$O$_3$/MWCNTs/Cellulose synthesis. The applied process in each stage is described in detail in SI, Sects. 2–1 to 2–5. Furthermore, all explanations concerning the characterization, adsorption experiments in the batch and continuous systems, adsorption isotherms and kinetic models, and thermodynamic parameters are widely presented in SI, Sects. 2–6 to 2–11.

2.6 Characterization of γ-Fe$_2$O$_3$/MWCNTs/cellulose

A vibrating sample magnetometer (VSM) (Lake Shore 7403) was used to measure the magnetic properties of the nanocomposites. The crystalline structure of the nanoparticles
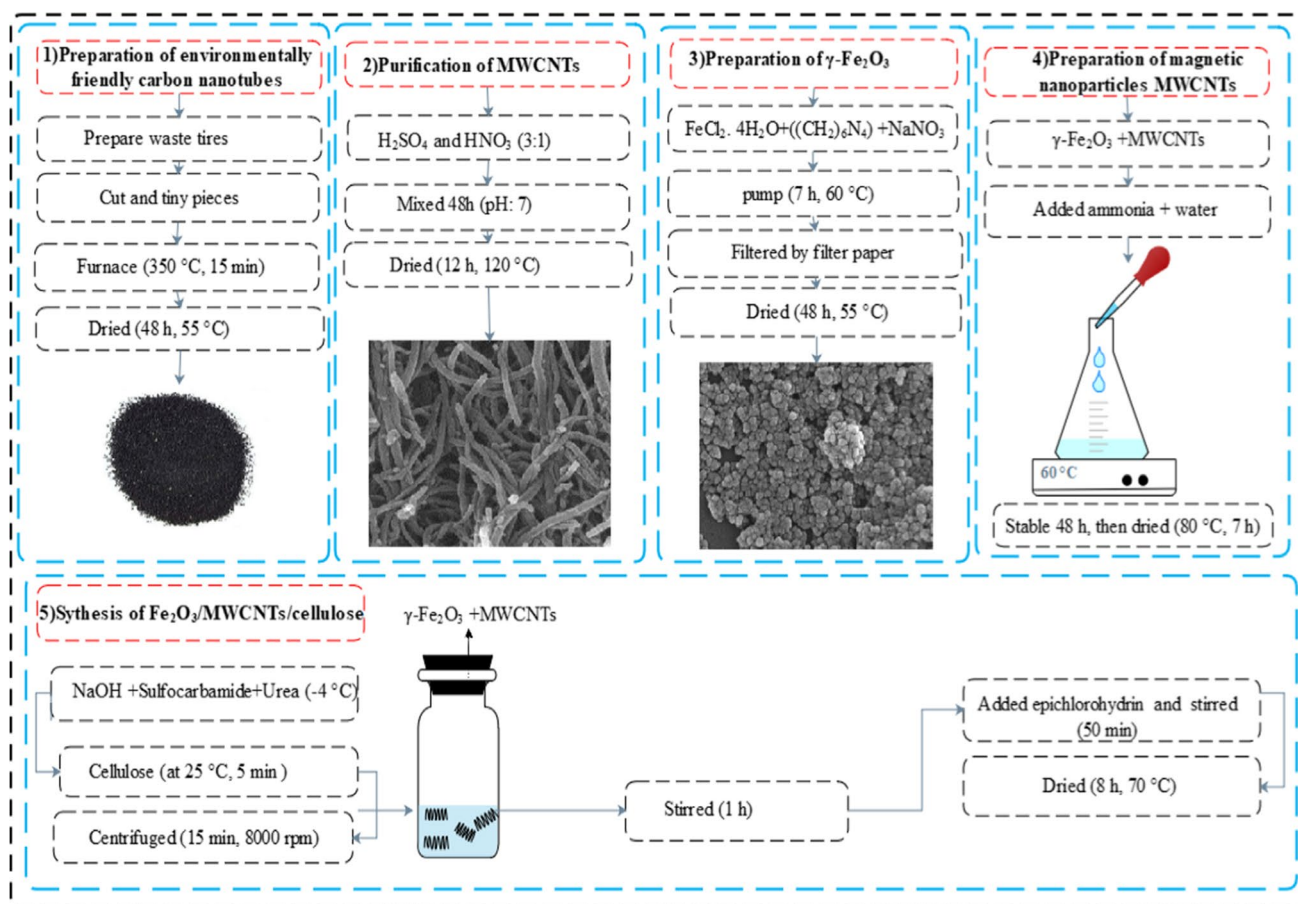
Fig. 1 Schematic diagram of the synthesis of γ-Fe₂O₃/MWCNTs/Cellulose

was measured using X-ray diffraction Rigaku MiniFlex 600 (XRD) using Cu Ka radiation (l = 0.15418 nm). The structure and morphology of the resulting composite nanoparticles were determined using Field Emission Scanning Electron Microscopy (FESEM) (TE-SCAN, MIRA3 FESEM model). Elemental analysis was performed using an alternating EDS spectrometer (FESEM). The zeta potential of the samples was also measured using a 3000HS Zetasizer. Fourier transforms infrared spectroscopy (Shimadzu, FTIR1650 spectrophotometer, Japan) with KBr plates was used to show the chemical nature of the prepared composites in the range of 4000–400 (cm⁻¹). Particle size distribution was recorded using the Dynamic Light Scattering (DLS) method using the Zetasizer 3000HS. The Brunauer–Emmett–Teller (BET) surface area of the samples was determined by nitrogen uptake (N₂) using a micrometer (Microtrac BEL Corp., Osaka, Japan). X-ray photoelectron spectroscopy (XPS) was performed (XPS VG, Esca Microprobe 2000 quantum physical electron, using Al Ka radiation) for chemical analysis and strength of the samples. The thermographic analysis (TGA) was measured using a Perkin Elmer (USA) device at 50 to 800 °C in atomic nitrogen.

2.7 Adsorption experiments in Batch system

Adsorption tests were performed in a batch system at room temperature and in glass containers using a thermostat shaker at a stirring speed of 150 rpm. Batch adsorption factors such as pH, contact time, adsorbent dose, initial concentrations of MG, and temperature were appropriately optimized to enable improved removal of MG from aqueous solution. For this purpose, 10 mg of catalytic adsorbent was added to 100 ml of contaminant solution and stirred continuously for 10 min at pH 7 and temperature of 313 K. Thereafter, the specimen was filtered using a Whatman grade 1 filter paper, and then the remaining adsorbate amount was measured via a spectrophotometer at 618 nm. The removal rate (R) and adsorption capacity q_t and q_e (mg/g) were calculated via the following equations [32]:

$$R = \frac{C_0 - C_{e,t}}{C_0} \times 100\% \tag{1}$$

$$R = \frac{C_0 - C_{e,t}}{C_0} \times 100\% \tag{2}$$

$$q_t = \frac{(C_0 - C_t)V}{m} \tag{3}$$

In these equations, C_0 is the initial concentration (mg/L), while C_e and Ct indicate the equilibrium (mg/L), and t time concentration of the pollutant, respectively. Q_t and q_e are respectively in terms of pollutant adsorption capacity in t (min) and equilibrium time. Also, V (L) is the volume of the adsorbent solution and m (mg) is the amount of adsorbent.

2.8 Adsorption isotherm models

To further evaluate the adsorption capacity, which is one of the most important parameters in the study of absorption systems, adsorption equilibrium isotherms are examined. Therefore, first, the relationship between the equilibrium concentration of MG after adsorption and the adsorption size on the adsorbent surface was investigated. Then, to understand the static adsorption behavior of MG pollutant by the γ-Fe$_2$O$_3$/MWCNTs/cellulose, Langmuir and Freundlich models were used. In this study, the Langmuir isotherm model is based on the assumption of monolayer adsorption from a homogeneous surface, inverse the Freundlich isotherm, which is considered multilayer adsorption on a heterogeneous surface. Linear and non-linear isotherm models are based on Eqs. (4 - 7) [33]:

Linear

$$\frac{C_e}{q_e} = \frac{1}{K_L q_m} + \frac{C_e}{q_m} \tag{4}$$

$$\ln q_e = \ln K_F + \frac{1}{n_F} \ln C_e \tag{5}$$

Nonlinear

$$q_e = \frac{q_m k_L C_e}{1 + k_L C_e} \tag{6}$$

$$q_e = k_F C_e^{1/n} \tag{7}$$

where q_m (mg/g) is the maximum absorption capacity and K_L (l/mg) is the Langmuir coefficient. K_F is the Freundlich equilibrium constant, which indicates the degree of adsorption capacity, and n_F is the heterogeneity factor that determines the strength of adsorption.

2.9 Investigation of the adsorption kinetics model

To investigate the relative adsorption kinetics, different kinetic models have been used. In this study, linear and non-linear pseudo-first-order and pseudo-second-order models were used to fit the kinetic data by the relationships expressed in the following functions [34]:

Linear

$$\ln(q_e - q_t) = \ln q_e - K_1 \tag{8}$$

$$\frac{1}{q_t} = \frac{1}{K_2 q_t^2} + \frac{1}{q_e} \tag{9}$$

Nonlinear

$$q_t = (q_e - e^{-k_1 t}) \tag{10}$$

$$q_t = \frac{k_2 q_e^2 t}{1 + k_2 q_e t} \tag{11}$$

where k_1 (min^{-1}) is the rate constant of pseudo-first-order and k_2 (g/mg/min) is the rate constant of pseudo-second-order. q_e (mg/g) and qt are the amount of species adsorbed by the adsorbent at equilibrium and at time t (min), respectively.

The intraparticle diffusion model was used to assay the probability of intraparticle diffusion resistance that may impact the adsorption process (Eq. (12)).

$$q_t = k_p t^{1/2} + I \tag{12}$$

where k_p and I respectively are the intraparticle diffusion rate constant and its intercept. The I, kp, and R^2 at different MG concentration values were measured from the linear plot of q_t versus $t^{1/2}$.

2.10 Investigation of thermodynamic parameters

By examining the changes in the amount of adsorption in terms of temperature, we can be explained whether the reaction is exothermic or endothermic. However, in addition to the optimum temperature, absorption constants, and equilibrium constants can be calculated from the slope of the curves. Therefore, thermodynamic parameters such as; entropy ($\Delta S°$) enthalpy ($\Delta H°$) and Gibbs free energy ($\Delta G°$) were assessed to determine the nature of pollutants by the adsorbent using the following equations [35]:

$$\Delta G° = \Delta H° - T\Delta S \tag{13}$$

$$\ln \frac{q_e}{C_e} = \frac{\Delta H°}{KT} + \frac{\Delta S°}{R} \tag{14}$$

where ΔH° (J/mol) is enthalpy changes and ΔS° (J/K.mol) is entropy changes, R is the gas constant (8.314 J/mol/K) and T is the temperature (K). The line diagram of $\ln q_e/C_e$ versus $1/T$ aided the measurement of ΔS° (J/K.mol) and ΔH° (J/mol) as the slope and intercept, respectively.

2.11 Experiments in the continuous system

The continuous experiments were performed in a glass column with an inner diameter of 3 cm, a height of 45 cm, and a volume of 150 mL. In this experiment, a peristaltic pump was used to maintain proper flow. The bottom of the glass column was covered with glass wool with a thickness of 0.06 cm to prevent the absorber from disappearing. The whole experiment was performed under optimal conditions. These experiments were performed with the optimal catalyst concentration and using an initial concentration of the solution containing a 5 mg/L of MG. In this study, the effects of process parameters such as flow rate (5, 10, and 15 mL/min), and bed height (3, 5, and 7 cm) were also investigated. Finally, samples were extracted at different time intervals from the bottom of the column, and the final concentration of MG was determined using a spectrophotometer. The volume of treated water, V_{eff} is measured via Eq. (15):

$$V_{eff} = Qt_{total} \tag{15}$$

where V_{eff} is the volume of treated water (ml), Q is the volumetric flow rate (ml/min), and t_{total} is the total flow time (min). The total amount of adsorbed dye (q_{total} (mg)) in the column studied is shown by the level under the plot of adsorbed dye concentration, which is determined using numerical integration in the following equation [36]:

$$q_{total} = \frac{QA}{1000} = \frac{Q}{1000}\int_0^T (C_0 - C_t)dt \tag{16}$$

In this equation, q is the total amount of dye absorbed (mg), Q is the flow rate of the solution (mL/min), A is the area under the breakthrough curve from C_0 to C_t (mg/min/L) from time 0 to any time t, C_0 is the influent dose (mg/L), and C_t is the effluent dose (mg/L) at time t (min). The total MG

dye entered into the column was calculated using Eq. 17 [37]:

$$m_{total} = \frac{C_0 Q t_{total}}{1000} \tag{17}$$

Meanwhile, R_{total} (%), the total dye adsorption, and CTEC (min), the contact time of empty column, were calculated via Eqs. (18 and 19), respectively [38]:

$$R_{total}(\%) = \frac{q_{total}}{m_{total}} \times 100 \tag{18}$$

$$CTEC = \frac{BEDVOLUME}{Q} \tag{19}$$

where Q is the flow rate (mL/min), t_{total} (min), and t_b (min) demonstrates saturation point and the time at breakthrough, respectively. V_b is the volume of treated water at breakthrough, and V_{total} is the total treated water.

The percentage of MG dye removal (mg) can be evaluated as the ratio of the absorbed MG mass (q_{total}) to the total mass of MG introduced into the column (m_{total}). The total MG uptake in the equilibrium (mg/g) condition is calculated using the following equation:

$$q_e = \frac{q}{m} \tag{20}$$

where the q_e is the total adsorption of MG in equilibrium (mg/g), q is the amount of adsorbed dye (mg/g), and m (g) is the mass of adsorbent.
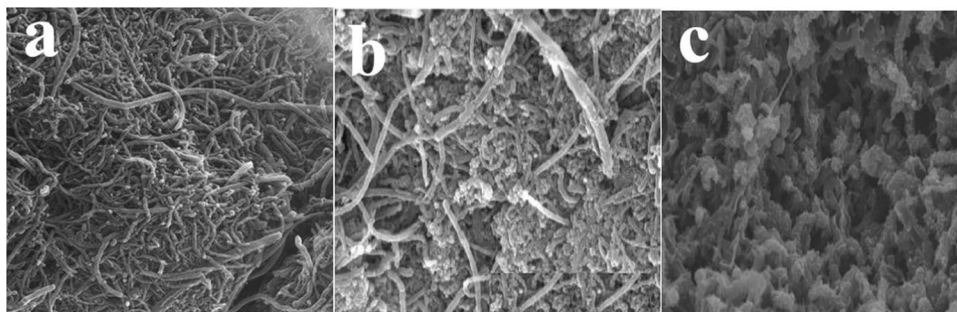
3 Results and discussion

3.1 Characterization of γ-Fe₂O₃/MWCNTs/Cellulose

3.1.1 Morphology and structure of γ-Fe₂O₃/MWCNTs/Cellulose

The surface morphology of γ-Fe₂O₃/MWCNTs/Cellulose was performed by FESEM analysis. As can be seen in Fig. 2a, the accumulated MWCNTs expanded a porous

Fig. 2 FESEM images of (a) MWCNTs, (b) γ-Fe₂O₃/MWCNTs, and (c) γ-Fe₂O₃/MWCNTs/Cellulose

network with entanglement. The image (Fig. 2b) clearly shows coated MWCNTs with nodules of γ-Fe_2O_3 nanoparticles that tethered on their sidewalls. Also, the γ-Fe_2O_3 has a homogeneous distribution on the tube. According to Fig. 2c, the γ-Fe_2O_3/MWCNTs/Cellulose magnetic nanoparticles have a non-uniform structure and indicate the presence of magnetic particles and MWCNTs attached to the cellulose surface. The addition of MWCNTs with their COOH functional groups to the blend is attended to lead to the constitution of hydrogen links between cellulose and MWCNTs [39]. The uneven and non-uniform surface of γ-Fe_2O_3/MWCNTs/Cellulose leads to an increase in adsorption active sites, which provides suitable conditions for the adsorption of MG onto the nanoparticle surface and thus, improves the adsorption rate [40].

The TEM electron microscopy images were used to study the structures of nanoparticles. As shown in Fig. 3a, the γ-Fe_2O_3 nanoparticles are spherical and have a diameter of about 70 nm. The surface of MWCNTs is uniform, and its average diameter is 52 nm (Fig. 3b). After cellulose coating and forming the γ-Fe_2O_3/MWCNTs/Cellulose nanoparticles, many spherical-shaped particles and hollow nanotube structures are observed. It can be clearly observed empty spaces and mesoporous structures in the structure of synthesized γ-Fe_2O_3/MWCNTs/Cellulose. For more detailed information, the EDS spectrum was examined to identify the elements present in the sample. As Fig. 3d indicates, the

signals of C, O, Fe elements were detected in the sample, which confirms the presence of magnetic nanoparticles in MWCNTs/Cellulose. These particles have a distribution of 120–170 nm with an average particle size of 44 nm, which is in close agreement with the obtained results by the TEM images (SI1).

and EDS spectrum of γ-Fe_2O_3/MWCNTs/Cellulose (d).

3.1.2 X-ray diffraction (XRD)

The crystalline structure of γ-Fe_2O_3/MWCNTs/Cellulose was analyzed using the XRD. As can be seen in Fig. 4, the diffraction peaks for the MWCNTs occurred at 2θ values of 26.53°, 35.5°, 50.94°, 63.25°, and 74.68°, respectively, typical for graphite carbon which correspond to the surface of crystals (002), (311), (102), (440), and (204) [41]. The diffraction peaks of 2θ at values of 30.42°, 35.5°, 43.82°, 54.35°, 57.64°, and 63.25° are belonged to (220), (311), (400), (422), (511) and (440) crystal planes of γ-Fe_2O_3, respectively. The XRD results are consistent with the JCPDS file NO # 19–629 [42]. The crystal structure of γ-Fe_2O_3/MWCNT composite can be confirmed by thin and sharp diffraction peaks. Therefore, it was revealed that γ-Fe_2O_3 nanocrystals do not change the MWCNT phases. For the γ-Fe_2O_3/MWCNTs/Cellulose, three additional peaks at 2θ values of 14.63°, 25.75°, and 34.40° belonging to cellulose

Fig. 3 TEM images of γ-Fe_2O_3 (**a**), γ-Fe_2O_3/MWCNTs (**b**), γ-Fe_2O_3/MWCNTs/Cellulose (**c**)
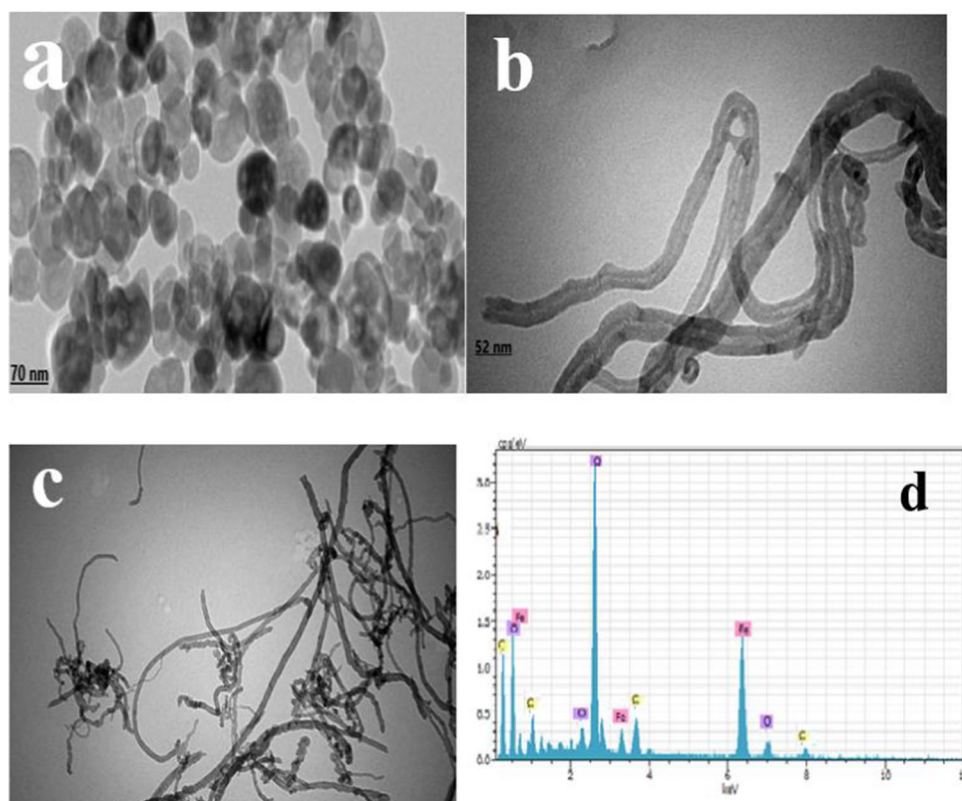
Fig. 4 XRD pattern of samples

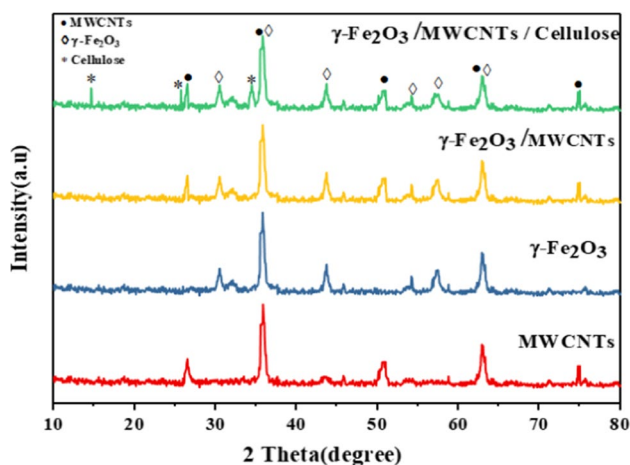**Fig. 5** FTIR spectra of samples

were observed, respectively, which correspond to the surface of crystals (101), (200), and (040) [43].

3.1.3 Magnetic properties Measurement of nanoparticles (VSM)

The magnetic properties of the samples were measured by the VSM analysis (SI2). As can be seen, the saturation magnetization value of γ-Fe$_2$O$_3$ was obtained (48.76) emu. g^{-1}, which after coating with MWCNT and cellulose led to a clear decline in the saturation magnetization value. The saturation magnetization values of γ-Fe$_2$O$_3$/MWCNTs and γ-Fe$_2$O$_3$/MWCNTs/Cellulose were measured about (32.47) and (22.38) emu.g^{-1}, respectively. The results of this analysis illustrated that the synthesized γ-Fe$_2$O$_3$/MWCNTs/Cellulose possessed an excellent super magnetism so that it can be separated from the solution using an external magnetic field. Therefore, the recovery of these magnetic nanoparticles plays a significant role in evaluating the accessibility of this bioadsorbent for water and wastewater treatment in practical terms [44].

3.1.4 Fourier Transforms Infrared Spectroscopy (FTIR)

The results of the FTIR spectrum for the functional group identification in synthesized γ-Fe$_2$O$_3$/MWCNTs/Cellulose in the range of 400–4000 cm^{-1} are shown in Fig. 5. The peak at 594 cm^{-1} is related to the vibrational tension of Fe–O in the Maghemite. Also, the absorption peaks in the range of 1106 to 1600 cm^{-1} confirm the presence of C-O and C=C in the composition. In addition, the peak at 3700 cm^{-1} is due to the OH tensile vibrations. The absorption peak at 1374 cm^{-1} corresponds to the tensile vibrations of O–H [19]. The absorption bands at 1628, 2922, and 1168 cm^{-1} were assigned to the tensile vibrations of C=C, C-H, and C-O
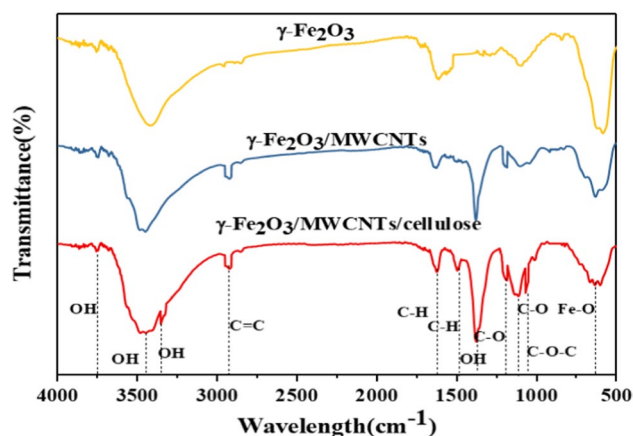
at MWCNTs [45]. After functionalization with cellulose, additional peaks at about 1427 cm^{-1} corresponded to the symmetric and asymmetric tensile vibrations of C-H [46]. The absorption bands at 1168 and 1054 cm^{-1} related to the C-O symmetric tensile vibrations, and the C–O–C skeletal vibrations in the pyranoid ring [40].

3.1.5 X-ray Photoelectron Spectroscopy (XPS)

The XPS analysis was used to investigate the composite surface conditions and to determine the atomic composition and bonding behavior of the material at the composite surface. Figure 6a indicates that the specimen contains C, O, and Fe, which are consistent with the results of the EDS data. The peaks of C1s at 289.3 eV are assigned to the carbon ester (O=C–O) (Fig. 6b). In addition, the Peaks at 287.5 eV and 286.6 eV arose of the bridging carbon (O–C–O) in the glucopyranose rings of the cellulose and C–O in the ester groups and cellulose [47]. The energy band peaks at 709.4 and 724.5 are related to the binding energies of Fe 2p$_{3/2}$ and Fe 2p$_{1/2}$ (Fig. 6c), respectively, which is assigned to γ-Fe$_2$O$_3$ [48]. In Fig. 6d, the binding energy of O1s is 533.1 eV, which corresponds to the typical binding energy of the C -O bond, which shows the dominant bond in the composition. While the peak at 530.9 and 536.6 eV is assigned to, C=O, and OH bonds [49, 50]. These XPS results showed that cellulose was bonded onto the carbon nanotubes through an esterification reaction [51].

3.1.6 Absorption–desorption analysis N$_2$

In this study, the N$_2$ adsorption-adsorption isotherm was used to assess the porosity and surface area of the synthesized nanoadsorbents in the relative pressure range of 0.5–0.5 and 70 °C (Fig. 7 and Table 1). Figure 7a illustrates that all N$_2$ Adsorption–desorption isotherms follow

Fig. 6 **a** Complete XPS scan spectrum of γ-Fe₂O₃/MWCNTs/Cellulose, **b**) C1s spectrum, **c**) Fe2p spectrum, and **d**) O1s spectrum
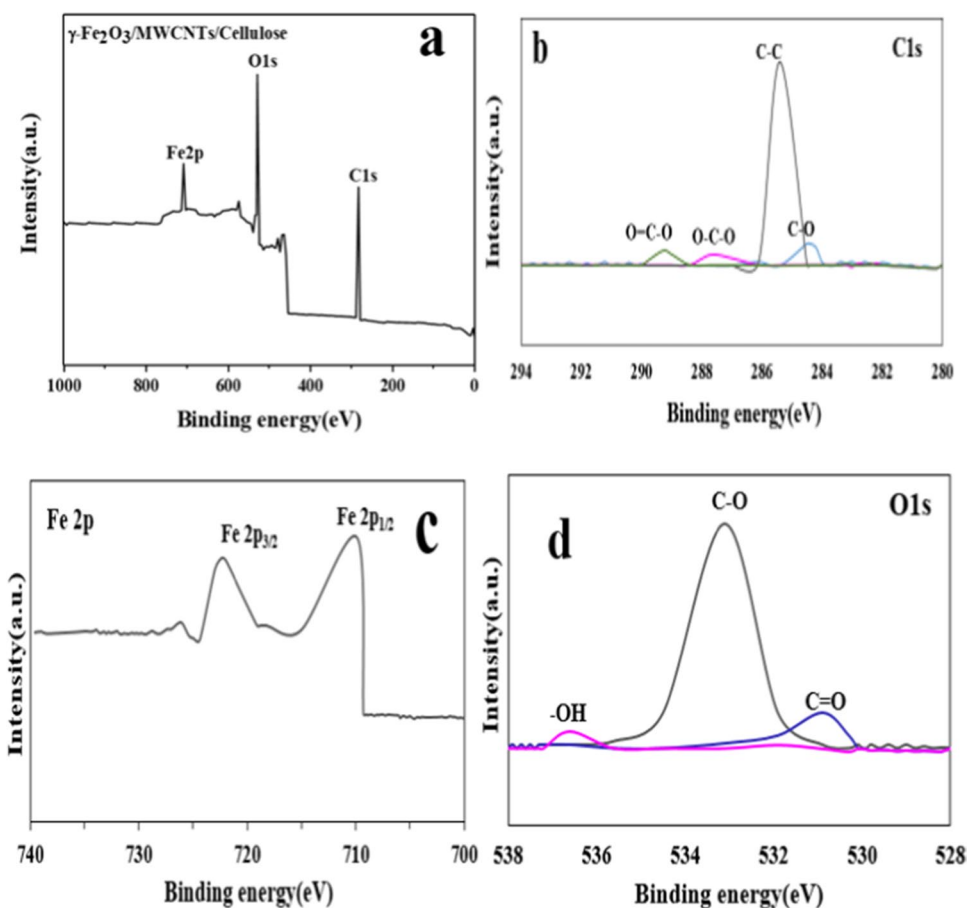
Fig. 7 **a**) N₂ adsorption–desorption isotherms; and **b**): pore size distribution of γ-Fe₂O₃, γ-Fe₂O₃/MWCNT, and γ-Fe₂O₃/MWCNT/Cellulose

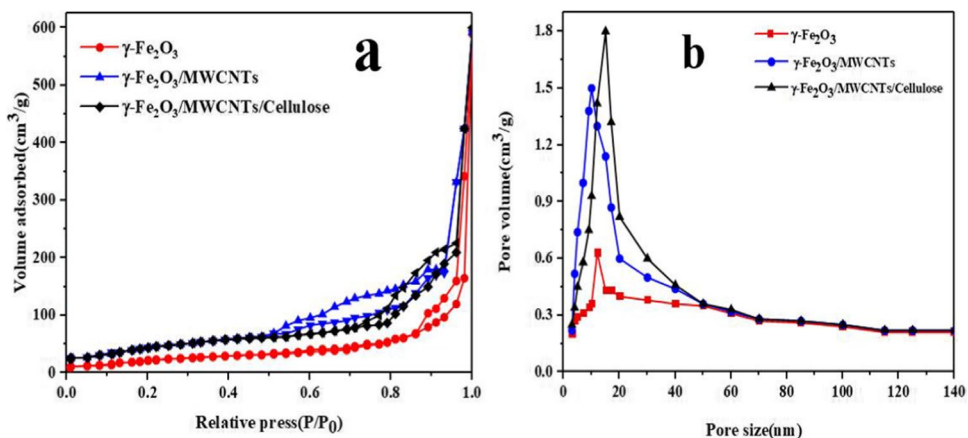**Table 1** BET analysis of synthesized nanoparticles

Sample	BET surface area (m^2/g)	Pore volume (cm^3/g)	Average pore size (nm)
γ-Fe₂O₃	42.11	0.423	11.02
γ-Fe₂O₃/MWCNTs	58.6	0.391	8.4
γ-Fe₂O₃/MWCNTs/Cellulose	132.27	0.388	7.83

the type V of IUPAC classification, indicating the existence of mico and mesopore cavities in the structure of synthesized samples with the mesoporosity domination [52]. According to Table 1, further modification from γ-Fe₂O₃ to Fe₂O₃/MWCNTs/Cellulose illustrates a positive effect on the nanomaterial surface area as favorable properties for adsorption. Furthermore, the Barrett-Joyner-Halenda

method was used to assay the pore volume distribution; the results are demonstrated in Fig. 7b. The average pore size was calculated at 11.02 nm, 8.4 and 7.83 nm for γ-Fe$_2$O$_3$, γ-Fe$_2$O$_3$/MWCNTs and γ-Fe$_2$O$_3$/MWCNTs/Cellulose, respectively (Table 1). Thus, the MWCNT coated with γ-Fe$_2$O$_3$ increases the ion transfer reaction rate at the electrode and electrolyte levels, which leads to improving catalytic and electrochemical properties [53]. Upon inclusion of the cellulose into the γ-Fe$_2$O$_3$/MWCNTs, the surface area increases while the average pore size and pore volume decrease. Therefore, it can be stated that both the peak pore volume and the average pore size are reduced after surface modification [54].

3.1.7 Thermal stability of the nanoparticles (TGA)

TGA analysis was utilized to distinguish the thermal analysis of nano-absorbent samples. As illustrated in Fig. 8, the thermal stability of γ-Fe$_2$O$_3$, γ-Fe$_2$O$_3$/MWCNTs, and γ-Fe$_2$O$_3$/MWCNTs/Cellulose nano-absorbents demonstrated some similar thermal behaviors, while there was no remarkable difference between the cure of γ-Fe$_2$O$_3$/MWCNTs and γ/Fe$_2$O$_3$/MWCNTs/Cellulose. Based on the results, The thermal stability curve for γ-Fe$_2$O$_3$ showed a dehydration weight loss of about 1.13% in the temperature range of 130–135 °C [55], and the major thermal decomposition phase of the γ-Fe$_2$O$_3$ was noticed in the temperature range 255–430 °C with a sharp weight loss of 82.35%. In the case of the γ-Fe$_2$O$_3$/MWCNTs/Cellulose, a dehydration weight loss (4.7%) was observed in the temperature range of 25–140 °C, then happened thermal stability up to 250 °C. The γ-Fe$_2$O$_3$/MWCNTs/Cellulose appeared a gradual weight loss of 77% in the temperature range of 170–397 °C. Regarding the γ-Fe$_2$O$_3$/MWCNTs and γ-Fe$_2$O$_3$/MWCNTs/Cellulose, the main weight loss started from 255 °C can be expressed as
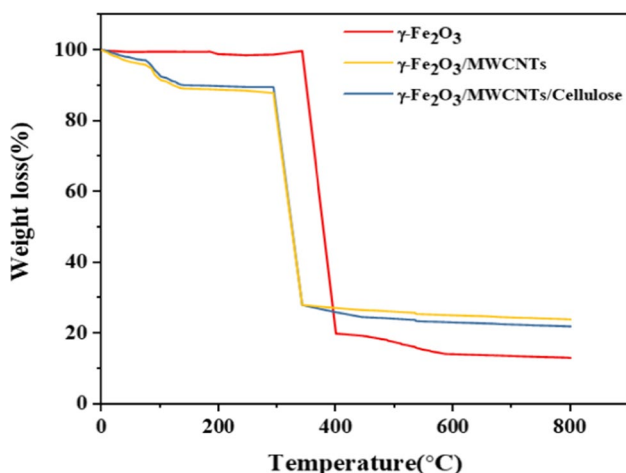

Fig. 8 Thermal stability curve of samples

the initiation of thermal degradation of cellulose contents and the main stage of decomposition of magnetic nanoparticles. It determined that the γ-Fe$_2$O$_3$/MWCNTs/Cellulose was initiated to decompose at a lower temperature (170 °C) than that of the γ-Fe$_2$O$_3$ (255 °C), which is attributed to the catalytic properties and heat absorption by γ-Fe$_2$O$_3$ [56].

3.2 The dye absorption performance in the batch system

3.2.1 Effect of pH on the MG adsorption process

Due to the interactions of metal ions and the adsorbents surface properties in an aqueous medium as well as, the separation of functional groups in adsorption sites, it is notable to investigate the effect of different pH of the solution (2–11) on MG adsorption using γ-Fe$_2$O$_3$/MWCNTs/Cellulose. The results showed that the highest adsorption effectiveness of MG occurred at pH 7 (SI 3a). It was found that the lowest adsorption capacity of MG was obtained equal to 47.33% at the pH = 2. The adsorption reduction in the acidic medium is due to the strong adsorption competition between the dye ions and the available highly positive H$^+$ in the medium for the occupation of the active adsorption sites. Therefore, the saturation of adsorbent by protons with a higher adsorption affinity significantly decreases its potential for MG adsorption. However, as the pH of the aqueous solution increases (pH > 7), the charge density at the surface gradually decreases[57]. Furthermore, the amount of MG dye adsorption increases by reducing the electrostatic repulsion between the charge of the positive dye molecule and the adsorbent surface. When the production of hydroxide functional groups in acidic pHs in the media increases, leading to produce a charge of negative on the adsorbent surface (SI 3b), so weak interaction or even repulsive force will occur between the dye molecule and the adsorbent surface, causing a decrement in the absorption rate [58, 59]. Likewise, the surface charge and electrophoretic performance of the γ-Fe$_2$O$_3$/MWCNTs/Cellulose nanoabsorbents were acquired to consider by the zeta potential analysis. As shown in Fig. S3c, the pH$_{pzc}$ of the γ-Fe$_2$O$_3$/MWCNTs/Cellulose nanoabsorbents is 6. Therefore, the surface of the γ-Fe$_2$O$_3$/MWCNTs/Cellulose is positively and negatively charged at pH$_{PZC}$ < 6 and pH$_{PZC}$ > 6, respectively. Thus, the amount of MG absorption increased by increasing the pH from 2 (47.33%) to 7 (89.68%). While from pH 7 to pH 11, the absorption rate was almost constant.

3.2.2 Effect of adsorbent dose on MG adsorption process

The amount of adsorbent dosage is an important factor that determines the amount of adsorbed adsorbate for the specified initial concentration. To investigate the dependence

of the MG removal to the adsorbent concentration, the effect of different concentrations of the adsorbent in the range of 0.03–0.15 g/l was evaluated while keeping other parameters constant in the adsorption process. As can be seen in SI 4a, the removal of MG increases with increasing the amount of adsorbent. It was evident that the removal of MG enhanced with the increment of nanoadsorbent concentration up to a certain percentage removal and then achieves a constant amount (absorption saturation limit). This increase in adsorption is due to the availability of more adsorption sites and limiting nanoadsorbent surfaces at high adsorbent concentrations. However, any further addition of the nanoadsorbent concentration more than 0.07 g/l does not cause much remarkable increase in the MG adsorption γ-Fe_2O_3/MWCNTs/Cellulose. This may be due to the saturation of adsorption sites as a result of excessive adsorbent particle accumulation [33]. Another reason is that, as the amount of adsorbent increases, the interaction between the adsorbent particles with the total surface area of the γ-Fe_2O_3/MWCNTs/Cellulose adsorbate decreases. The obtained results are consistent with several previous studies [60–62] who confirmed that the removal of the dye increased with increasing adsorbent increases.

3.2.3 Effect of initial concentration of MG dye on the adsorption process

The initial concentration of the contaminant plays a key role in the absorption of the contaminant. Therefore, in this study, the initial MG concentration was varied (5–100 mg/L) while keeping the other factors constant (pH 7, the adsorbent concentration of 0.07 g/L at 313 K). The results showed (SI 4b) that the adsorption efficiency of dye from an aqueous solution increases, with increasing contact time. For different initial concentrations of MG, the adsorption intensity was quick at the beginning and slowed down as adsorption time enhanced. The removal efficiency reduced from 92.41 to 57.39% with an initial enhancement of MG concentration from 5 mg/L to 100 mg/L. The increase in adsorption at low concentrations of pollutants is due to the fact that the dye molecule has a strong affinity to the surface of the adsorbent. In this condition, the number of MG molecules accessible in the solution was low as compared to the accessible adsorption sites on the γ-Fe_2O_3/MWCNTs/Cellulose, therefore the MG molecules are adsorbed by particular active sites, resulting in a higher amount of removal of MG [63, 64]. In other words, this phenomenon is attributed to most empty adsorption sites which are accessible for adsorption at the initial step, over time, the remaining vacant surface sites are hard to be filled due to repulsive forces between the dye molecules on the absorbent solid phases [12].

3.2.4 Effect of contact time on the MG adsorption process

Determination of the equilibrium time is one of the most important properties that indicate dye adsorption on nanoadsorbent. SI 4c shows the effect of dye adsorption time by nanoadsorbent. Results showed in SI 4c demonstrate the highest adsorption at 90 min and then equilibrium achievement. the highest adsorption attained at 90 min has been found to be 74.45%. With a further enhancement in time, the percent adsorption remained approximately the same. It seems that a time of 90 min can be the equilibrium point of dye adsorption MG with nanoadsorbent. Because at this time the highest amount of dye adsorption has been observed. Therefore, the dye adsorption equilibrium time is determined at 90 min.

3.2.5 Effect of temperature on the MG adsorption process

The change in sample temperature affects the adsorption process by changing the solubility of the adsorbent and the molecular bonds. Therefore, the effect of temperature on MG dye adsorption using γ-Fe_2O_3/MWCNTs/Cellulose was investigated at different temperatures (298–323 K), and the results are shown in Fig. S4d. The results showed that the highest percentage of MG adsorption was obtained at the temperature of 313 K. Thus, increasing the temperature leads to the adsorption of MG by γ-Fe_2O_3/MWCNTs/Cellulose nanoparticles. This result indicates that the process is an endothermic reaction, which decreased the viscosity of the solution. This process also leads to an enhancement in the external mass transfer and the diffusion of dye molecules into the pores of the adsorbent. In other words, increasing the temperature leads to the mobility of the dye molecule and increases the interactions between the absorption and the adsorbent or the creation of new active sites on the adsorbent.

3.2.6 Investigation of equilibrium adsorption isotherm

The equilibrium adsorption isotherm was evaluated at different concentrations (5–100 mg/L) of MG under optimal conditions using γ-Fe_2O_3/MWCNTs/Cellulose magnetic nanosorbents at pH 7 for 150 min. To evaluate the interactive behavior between MG and γ-Fe_2O_3/MWCNTs/Cellulose, the Langmuir and Freundlich isotherm models were used to match correlation data in MG adsorption, and the results are shown in SI 5. As can be seen, the enhanced MG adsorption capacity was showed with enhancing adsorbent concentration 5–100 mg/l. The noticed proportional enhance in adsorption capacity with adsorbent concentration rise could be ascribed to the enhanced surface area of the adsorbent and the accessibility of adsorption sites. Table SI 1 presents the isotherm parameters of

the Langmuir and Freundlich models and the correlation coefficient (R^2). Accordingly, the correlation coefficients (R^2) for Langmuir and Freundlich models were obtained at 0.9835 and 0.95, respectively. The maximum adsorption capacity of MG in the adsorbent predicted by the Langmuir model was 47.61 mg/g. Furthermore, a constant rate of 2.69 mg/g was obtained. In the Langmuir model, the surface is assumed to be homogenous and there is no interference between molecules adsorbed by the MG contaminant on the adsorbent nanoparticles. Thus, the MG adsorption on γ-Fe$_2$O$_3$/MWCNTs/Cellulose should be affected by a monolayer [65]. The Freundlich model assumes a multilayers adsorption with non-uniform distribution of adsorbents. The amount of n, which has been defined in the range of 1–10, illustrates the adsorption of MG contaminants on γ-Fe$_2$O$_3$/MWCNTs/Cellulose nanosorbents [35]. Also, the value obtained from the n_F parameter, which is related to the adsorption intensity, indicates that the adsorption process has occurred physically and is favorable. As a result, the Langmuir model was better than the Freundlich model for explaining the adsorption isotherm of MG in the adsorbent. In this study, the nonlinear regression method was also investigated and showed a significant difference between the nonlinear and the linear method (SI 5c, d) and according to Table S1, the correlation coefficients R^2 values were gained for the Langmuir and Freundlich isotherms as 0.95 and 0.94, respectively. It was observed that in the nonlinear isotherm, the Langmuir model is more suitable than the Freundlich model. According to the values of correlation coefficient (R^2), the Langmuir model is suitable for investigating the removal of dyes by nanocomposites. Thus, it can be considered that the adsorption sites are homogeneously placed on the prepared nanocomposite and the adsorption process is uniformly performed. Also, based on the results of comparing two models of linear and nonlinear regression, it was clearly found that linear regression is more suitable for determining isothermal parameters [66].

The Temkin isotherm considers Interactions between the adsorbent-adsorption. The expressed by equation is as follows:

qe = BlnA + BlnCe

where Ce is the concentration of adsorbate in solution at equilibrium (mg/L), qe is the amount of adsorbate adsorbed at equilibrium (mg/g); b is the Temkin constant (J/mol), B is a constant relevant to the heat of adsorption that is expressed by the expression B = RT/b, T is the absolute temperature (K), R is the gas constant (8.314 J/ mol K), and A is the Temkin isotherm constant (L/ g). From the plot of qe vs. lnCe, B and A can be determined from the slopes (B) and intercepts (BlnA) respectively.

Isotherm constants for Temkin isotherm mentioned above were calculated from the linear isotherm figure for different MG concentrations. SI 5 shows the Temkin isotherm for MG dye.

3.2.7 Evaluation of adsorption kinetics

To investigate the adsorption rate and calculate the relevant constants, pseudo-first and pseudo-second kinetic models were used. For this purpose, curves related to the adsorption time of dye contaminants were performed by γ-Fe$_2$O$_3$/MWCNTs/Cellulose magnetic adsorbents for 150 min. The related results are presented in SI 6 and Table S2. The nonlinear and pseudo-second-order kinetic models revealed the higher regression coefficients (R^2) for all MG dye concentrations in this study, indicates a better fit of this model with the experimental isotherms. In light of these results can be concluded that the adsorption of MG using γ-Fe$_2$O$_3$/MWCNTs/Cellulose is more affected by chemical adsorption behavior [67, 68].

3.2.8 Investigation of adsorption thermodynamic

To further investigate the adsorption of MG using γ-Fe$_2$O$_3$/MWCNTs/Cellulose magnetic nanoparticles, thermodynamic parameters were examined and presented in Fig. S7 and Table S3. $\Delta H°$ (kJ/mol) demonstrates the strength of binding interactions and considers the change of the equilibrium adsorption with the temperature at constant coverage. The value of $\Delta H°$ to determine the amount of MG adsorption onto γ-Fe$_2$O$_3$/MWCNTs/Cellulose was obtained from the slope of the plot of lnK$_d$ versus 1/T, as shown in SI 7. The negative slope clearly confirms that the adsorption process is exothermic in nature [69]. Besides, the obtained negative Gibbs energy ($\Delta G°$) at different temperatures (Table S3) indicates the spontaneous MG adsorption by the γ-Fe$_2$O$_3$/MWCNTs/Cellulose adsorbent. In other words, the decrement trend of $\Delta G°$ values with increasing temperature indicates more affinity of adsorption at higher temperatures. Furthermore, the obtained values for $\Delta G°$ can be used to understand more about the mechanism of the adsorption process as the ranges of zero to -20 kJ mol^{-1},—20 to -80 kJ mol^{-1}, and -80 to -400 kJ mol^{-1} indicate the physical adsorbent, physical and chemical adsorption together, and chemical adsorption, respectively. Regarding this, the reaction between MG molecules and γ-Fe$_2$O$_3$/MWCNTs/Cellulose follows a chemical mechanism in most cases [12]. However, the positive value of entropy system ($\Delta S°$) equal to 37.67 J mol k $^{-1}$can be attributed to the increase in irregularity, indicating the adsorbent collisions and MG molecules are in line with system irregularities [70].

3.2.9 Reusability

The recovery of synthesized nanoparticles is very important to validate the economic stability of the nanoadsorbent as well as decrease residual waste. Excellent adsorption recovery alters the adsorption process into an economic process. Therefore, in this study, the reusability of magnetic nanoparticles was evaluated via adsorption–desorption trials. Therefore, at each step of MG dye adsorption, the resulting nanoparticles were extracted from the treated solution using a magnetic field and washed with distilled water, NaOH and HCl (0.1 mm), and NaCl (0.1 mm), respectively. Hence, the MG desorption test was performed with four different wash treatments and the results showed that when NaOH was used as the eluent, the washing rate of MG achieves 87.35%. While the application of acidic media demonstrated a low desorption rate of the adsorbent (Fig. 9a). Regarding this, it can be stated that in alkaline media, due to the reduction of electrostatic repulsion between the dye with a positive charge and the adsorbent surface with a negative charge, the amount of dye absorption was higher [71]. Therefore, the rehabilitation of the Fe_2O_3/MWCNTs/Cellulose into alkaline media is possible. Thus, in the subsequent adsorption/desorption cycles of MG, NaOH solution (0.1 M) was used. The results showed that the performance of nanoparticles is almost constant and there is no significant decrease in MG adsorption up to 4 cycles Fig. 9b. After 4 recycles using the adsorbent, MG adsorption declined from 92.41% in the first stage to 81.38% in the fourth stage. The reduction of adsorption behavior may be ascribable to the protonation of the adsorption sites and weakening of continuously applied functional groups. The noticed negligible decrease in adsorption capacity may also be attributed to the agglomeration of dye ions in the stacked tubular
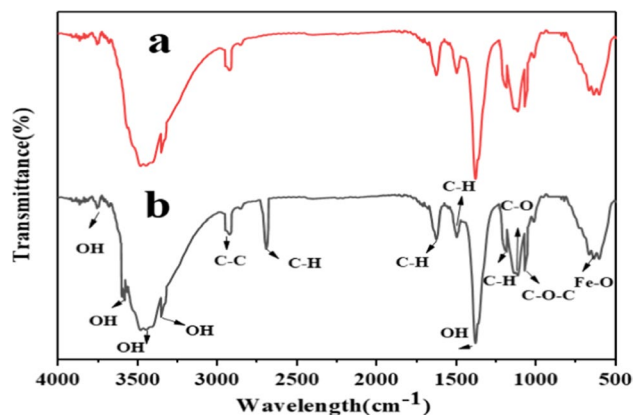

Fig. 10 FTIR spectra of γ-Fe_2O_3/MWCNTs/Cellulose before and after recycling test

structures hindering MG ions further availability to the binding sites. Therefore, the γ-Fe_2O_3/MWCNTs/Cellulose has good adsorption capacity and can be used in a practical, relatively stable, and inexpensive way in several cycles without a significant reducing performance.

However, FTIR results of γ-Fe_2O_3/MWCNTs/Cellulose nanoadsorbent were used after four recycles. FTIR analysis of nano adsorbent was carried out before and after MG adsorption (Fig. 10). Based on Fig. 10, much difference was not depicted between the two FTIR patterns. Considering Fig. 10, the additional peaks of peak 2695 cm^{-1} pertained to C–H vibrations, whereas peaks 3556 cm^{-1} pertained to O–H stretching vibrations in the fourth reuse. As noticed much variation did not occur in the FTIR curve peaks before and after the adsorption process. This result respected that γ-Fe_2O_3/MWCNTs/Cellulose nano-adsorbent had excellent chemical stability and can safely be applied as a reusable adsorbent in most of the applications.

Fig. 9 **a** Adsorption of MG by γ-Fe_2O_3/MWCNTs/Cellulose using different elution solutions and **b**) Absorption/desorption cycle using NaOH as eluent
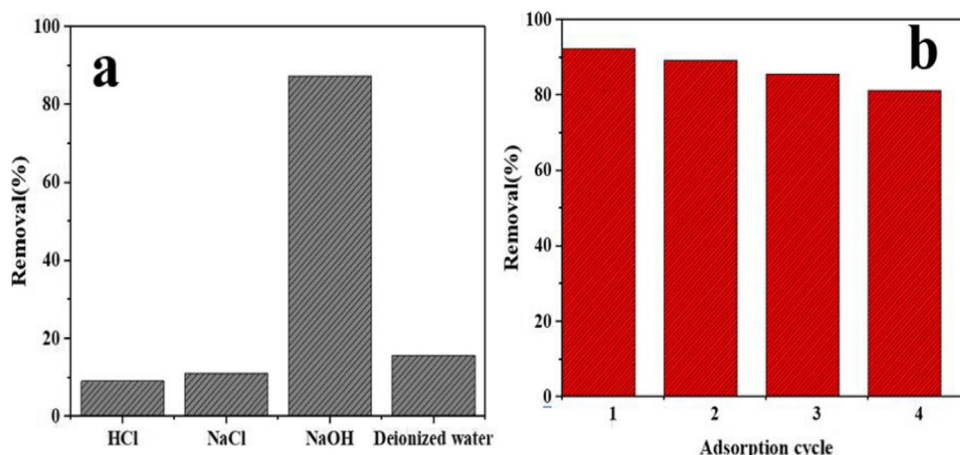
3.3 Adsorption performance in a continuous system

3.3.1 Effect of flow rate on the MG adsorption process

Breakthrough curves of MG dye adsorption on adsorbent γ-Fe_2O_3/MWCNTs/Cellulose at different flow rates (3, 5, 7, 9 mL/min) were examined in the optimal parameters obtained in the batch system and at a bed height of 4 cm. The results showed that by increasing the flow rate from 3 to 9 ml/min, the dye adsorption by the adsorbent reduced from 91.25 to 67.84% (SI 8a). The volume of water treated (V_{eff}) also decreases as the flow rate enhances. The reason for removal efficiency decrease with increasing flow rate is due to the decrease in contact time between the adsorbent and the dye molecules which do not permit complete saturation of the adsorbent active sites by dye molecules, and eventually lead to a reduction in the amount of dye molecule adsorbed. Therefore, it can be stated that the adsorption of dye molecules is dependent on the flow rate. However, at low flow rates from 9 to 3 ml/min, the availability of adsorbents and dyes increases, and the sorption of MG molecule enhances steadily and there is a delay in the saturation of the sorbent [37]. Therefore, the lower flow rates are preferred to achieve a greater MG adsorption efficiency. These results are in close agreement with the previous findings [4, 36].

3.3.2 Effect of different bed heights on MG adsorption process

In this study, the effect of different bed heights (2, 4, 8, 10 cm) towards MG absorption with a flow rate of 3 ml/min, dye concentration (5 mg/L), adsorbent (0.07 g/L), and pH 7 was performed, and the results are shown in SI 8b. As observed, the reaction breakthrough curves in dye adsorption by γ-Fe_2O_3/MWCNTs/Cellulose indicated the highest adsorption at high bed height. The reason for this is that the enhancement of the bed height increases the time for breakthrough and exhaustion [65]. In other words, raising

the bed height leads to an increase in the amount of adsorbent, thereby creating more active adsorption sites for MG dye adsorption, resulting in an availability of a long time of the interaction between the adsorbent and dye, which leads to increased dye adsorption [72].

The impact of parameters in the breakthrough curves for the adsorption of MG by the nanoadsorbent in Table S4 indicated that with raising influent MG concentration, the speed of saturation and the breakthrough time decrease. However, by reducing MG concentration, later breakthrough curves form. Therefore, the highest treated volume was obtained at the lowest influent dye concentration. Also, the adsorption capacity is enhanced by raising the influent dye concentration. Therefore, it can be stated that in the higher concentration, the created gradient leads to a faster transport due to mass transfer coefficient or an enhanced diffusion coefficient [73]. Accordingly, the maximum adsorption capacity was obtained at a concentration of 5 mg/L, 10 cm of bed height, and 3 mL/min of flow rate (Table S5). With increasing the influent dye concentration from 5 to 100 mg/L, the adsorption and total dye absorbed increased from 4.54 to 27 mg/g and 1.8 to 76.5 mg, respectively. This increase may be due to the high influent dye concentration, which leads to an increase in the driving force for the transfer process to overcome the resistance to mass transfer [73]. As the influent dye concentration enhanced from 5 to 100 mg/L, the exhaust time decreased from 120 to 85 min. The results of this study showed that higher initial influent concentrations lead to a higher driving force for mass transfer, therefore the adsorbent saturates more rapidly, which reduces the exhaust time and the length of the adsorption region [74].

3.4 Comparison of MG adsorption with other studies

The MG dye adsorption capacity acquired by the γ-Fe_2O_3/MWCNTs/Cellulose nanoabsorbent in this study was compared with previous studies as indicated in Table 2. As can

Table 2 Comparison of the adsorption capacity of the reported adsorbents in the MG dye sorption

Adsorbent	Adsorbate	q_m (mg/g)	pH	t(min)	Isotherm/kinetics	Ref
Ni_xZn_x–XFe_2O_4	MG	67	6	120	L/PSO[3]	[75]
Halloysite nanotubes (HNTs)	MG	99.6	9.5	30	L/PSO	[76]
$CuFe_2O_4$	MG	22	7	30	L/PSO	[77]
Magnetic Nickel Oxide	MG	87.72	7	30	L/PSO	[71]
bentonite (BT)	MG	188.68	11	60	L/PFO[4]	[78]
Thiolated GO[1]	MG	40.5	7	60	L/PSO	[79]
Aniline/indole copolymer	MG	434	8	20	L/PSO	[80]
GO	MG	27.16	3	100	L/PSO	[81]
rGO	MG	13.52	3	100	L/PSO	[81]
γ-Fe_2O_3/MWCNTs/Cellulose	MG	47.61	7	90	L/PSO	This study

[1]Graphene Oxide, [2]Langmuir, [3]Pseudo-Second Order, [4]Pseudo-First-Order kinetic.

be observed, the γ-Fe$_2$O$_3$/MWCNTs/Cellulose demonstrated a good adsorption capacity compared to the adsorption capacities of different nanoabsorbents from other studies. It should be highlighted that although the adsorption capacity by the γ-Fe$_2$O$_3$/MWCNTs/Cellulose is rather low compared to some of the previous investigations, the applied precursor to synthesis the γ-Fe$_2$O$_3$/MWCNTs/Cellulose in the present study is more eco-environmentally friendly in comparison with those from a practical application perspective. However, the higher adsorption capacity can be assigned to the high surface area and functional groups present in the γ-Fe$_2$O$_3$/MWCNTs/Cellulose, which provided great binding sites for MG dye adsorption. Therefore, the γ-Fe$_2$O$_3$/MWCNTs/Cellulose can be proposed as a promising adsorbent for the adsorption of MG dye from aqueous media, because it has a relatively good adsorption capacity and can be easily extracted from treated effluents using a magnetic field.

3.5 Adsorption Mechanism of MG

Recently, adsorption has become one of the principal techniques of dye removal and the investigation of adsorption mechanisms of dye pollutants by adsorption kinetics and adsorption thermodynamics has become the main focus of research. The kinetic for MG adsorption process by some nano-adsorbents is faster than other adsorbents, which makes them favorable for the adsorption of dye molecules [57]. The adsorption factors of MG by different adsorbents are shown in Table 2. As can be seen, the adsorption mechanisms by different adsorbents in MG dye adsorption are mostly consistent with the PSO kinetic model, which shows that the dye adsorption mechanism is performed by adsorption using chemical adsorption. The adsorption mechanisms by nano-absorbents were mostly in correspondence with the PSO kinetic model, demonstrating that the adsorption of MG via these sorbents occurs by chemical adsorption. Due to the heterogeneity of the nano-adsorbent surface, some adsorption isotherm corresponds to the Langmuir isotherm and some others to the Freundlich isotherm. Additionally, the majority of nano-adsorbents pursue the Langmuir isotherm model higher than the Freundlich model. When it comes to comparison, the appropriate isotherm model for other nano-adsorbents is divided into those Freundlich and Langmuir. Table 2 indicates the proportion of each isotherm and kinetic model in all the nano-adsorbents studied. This clearly can represent that nano-adsorbents have a homogenous surface and MG molecules are adsorbed as monolayers. also, another method of surveying the adsorption process is the surface attributes of nano-adsorbent and its compatibility with the structure of adsorbate (dyes) to make an efficient adsorption process. In the adsorption process, there are various mechanisms such as hydrogen bonds, van der Waals and electrostatic interactions, non-covalent interactions, and ion

exchange, on which adsorption–desorption depends. Therefore, the predominant adsorption processes depend on the functional groups bonded on the surface of the adsorbent. One study focusing on ion exchange resins for reactive two dyes removal showed the importance of electrostatic interaction and also surface functional groups [82]. MG dye contains triphenylmethane in its structure, so it is a cationic dye. So, the surface charge of nanoadsorbent plays the main role in the process in different pH conditions. This dye has a different quantity of cationic groups (triphenylmethane) which varies the charges available on the surface in both acidic and basic solutions. This was studied that the pH value of 7.0 contributed to the high adsorption which shows that the electrostatic interaction between the major groups in MG and the functional groups on the surface of nanoadsorbent is the dominant mechanism[83].

Results indicates that the rate first increased up to 7 and then decreased to 8, thus, working pH was found to be 7. The efficiency of adsorption of the nano-adsorbent initially improved with the initial upsurge in pH value due to the ionization of the hydrophilic adsorbent. The properties of FTIR indicate the presence of carboxyl, hydroxyl and amide groups, which are known as active sites in nanoadsorbent to adsorb MG ions from the aqueous solution. This favored the intermolecular interactions among the MG ions and nanoadsorbent[84].

4 Conclusion

As a solutions-oriented strategy in battling with the increasing trend of the waste tire in the world, the waste tire and cellulosic precursor were applied to synthesize the highly stable and generable nanoabsorbent i.e. γ-Fe$_2$O$_3$/MWCNTs/Cellulose. It was synthesized through a chemical vapor deposition method to remove MG from aqueous solutions in both batch and continuous. To identify the characteristics of prepared nanoabsorbent, a wide range of analyses including XRD, FESEM, EDX, TEM, EDS, DLS, FTIR, VSM, BET, XPS, and TGA were employed. The amount of dye adsorption increased with decreasing flow rate and enhancing column length from 9 to 3 mL/min and 2 to 10 min, respectively. The results of this study showed that the removal rate increased with increasing the concentration of γ-Fe$_2$O$_3$/MWCNTs/Cellulose up to 0.07 g/L and then decreased with a further increase of adsorption. Furthermore, in the continuous system, the adsorption potential of γ-Fe$_2$O$_3$/MWCNTs/Cellulose was increased by the decrement of flow rate and the increment of bed height. The pseudo-second-order and the Langmuir model were the best kinetic and isothermal models to describe the MG adsorption process ($R^2 > 99\%$). The thermodynamic results demonstrated that the adsorption process is exothermic and spontaneous. In light of the

reusability experiment, the MG adsorption efficiency was disclosed to no notable decrease even after four successive adsorption cycles as an important parameter from a practical perspective. The MG ions can merely be adsorbed onto the surface of the nanoadsorbent via physicochemical interactions. In conclusion, the current study demonstrates that the γ-Fe_2O_3/MWCNTs/Cellulose synthesized from waste tire and cellulosic material can be proposed to manufacture an eco-environmentally friendly adsorbed in the context of water and wastewater treatment.

Author contribution Mansooreh khalatbary: Writing, original draft, Data curation, Methodology. Mohammad Hossein Sayadi: Supervision, Methodology, Validation, Writing—review & editing. Mahmoud Hajiani: Visualization, Conceptualization, Investigation. Mohsen Nowrouzi: original draft, Data curation, Methodology, Validation, Writing—review & editing.

Declarations

Conflicts of interest The authors declare no conflict of interest.

References

1. Poorsajadi F, Sayadi MH, Hajiani M, Rezaei MR (2020) Synthesis of CuO/Bi_2O_3 nanocomposite for efficient and recycling photodegradation of methylene blue dye, International Journal of Environmental Analytical Chemistry, 1–14. https://doi.org/10.1080/03067319.2020.1826464

2. Das P, Debnath P, Debnath A (2021) Enhanced sono-assisted adsorptive uptake of malachite green dye onto magnesium ferrite nanoparticles: kinetic, isotherm and cost analysis. Environmental Nanotechnology, Monitoring & Management 16:1005506

3. Syed S (2011) Study of the removal of malachite green from aqueous solution by using solid agricultural waste. Res J Chem Sci 1:1–14

4. Ahmadpour N, Sayadi MH, Sobhani S, Hajiani M (2020) A potential natural solar light active photocatalyst using magnetic $ZnFe_2O_4@TiO_2$/Cu nanocomposite as a high performance and recyclable platform for degradation of naproxen from aqueous solution. J Clean Prod 268:122023. https://doi.org/10.1016/j.jclepro.2020.122023

5. Kushwaha AK, Gupta N, Chattopadhyaya M (2010) Enhanced adsorption of malachite green dye on chemically modified silica gel. J Chem Pharm Res 2:34–45. https://doi.org/10.1080/19443994.2013.803319

6. Das P, Debnath A (2021) Reactive orange 12 dye adsorption onto magnetically separable CaFe2O4 nanoparticles synthesized by simple chemical route: kinetic, isotherm and neural network modeling. Water Practice & Technology 16:1141–1158

7. Sayadi MH, Ahmadpour N, Homaeigohar S (2021) Photocatalytic and Antibacterial Properties of Ag-$CuFe_2O_4$@WO_3 Magnetic Nanocomposite. MDPI 11:298. https://doi.org/10.3390/nano11020298

8. Sharma G, Kumar A, Naushad M, Thakur B, Vo D-VN, Gao B, Al-Kahtani AA, Stadler FJ (2021) Adsorptional-photocatalytic removal of fast sulphon black dye by using chitin-cl-poly (itaconic acid-co-acrylamide)/zirconium tungstate nanocomposite hydrogel. J Hazard Mater 416:125714. https://doi.org/10.1016/j.jhazmat.2021.125714

9. Sharma G, Pathania D, Naushad M, Kothiyal N (2014) Fabrication, characterization and antimicrobial activity of polyaniline Th (IV) tungstomolybdophosphate nanocomposite material: efficient removal of toxic metal ions from water. Chem Eng J 251:413–421. https://doi.org/10.1016/j.cej.2014.04.074

10. Sharma G, Naushad M, Pathania D, Mittal A, El-Desoky G (2015) Modification of Hibiscus cannabinus fiber by graft copolymerization: application for dye removal. Desalin Water Treat 54:3114–3121. https://doi.org/10.1080/19443994.2014.904822

11. Zhuang Y, Liu J, Chen J, Fei P (2020) Modified pineapple bran cellulose by potassium permanganate as a copper ion adsorbent and its adsorption kinetic and adsorption thermodynamic. Food Bioprod Process 122:82–88. https://doi.org/10.1016/j.fbp.2020.04.008

12. Zadeh RJ, Sayadi MH, Rezaei MR (2021) Synthesis of Thiol modified magMCM-41 nanoparticles with rice husk ash as a robust, high effective, and recycling magnetic sorbent for the removal of herbicides. J Environ Chem Eng 9:104804. https://doi.org/10.1016/j.jece.2020.104804

13. Deb A, Debnath A, Bhowmik K, Rudra Paul S, Saha B (2021) Application of polyaniline impregnated mixed phase Fe_2O_3, $MnFe_2O_4$ and ZrO_2 nanocomposite for rapid abatement of binary dyes from aqua matrix: response surface optimisation. Int J Environ Analytical Chem, 1–19

14. Das P, Nisa S, Debnath A, Saha B (2020) Enhanced adsorptive removal of toxic anionic dye by novel magnetic polymeric nanocomposite: optimization of process parameters. Journal of Dispersion Science and Technology, 1–16

15. Deb A, Debnath A, Saha B (2021) Sono-assisted enhanced adsorption of eriochrome Black-T dye onto a novel polymeric nanocomposite: kinetic, isotherm, and response surface methodology optimization. J Dispersion Sci Technol 42:1579–1592

16. Hoyos-Palacio LM, Castro DPC, Ortiz-Trujillo IC, Palacio LEB, Upegui BJG, Mora NJE, Cornelio JAC (2019) Compounds of carbon nanotubes decorated with silver nanoparticles via in-situ by chemical vapor deposition (CVD). J Market Res 8:5893–5898. https://doi.org/10.1016/j.jmrt.2019.09.062

17. Anis B, Mostafa A, El Sayed Z, Khalil A, Abouelsayed A (2018) Preparation of highly conductive, transparent, and flexible graphene/silver nanowires substrates using non-thermal laser photoreduction. Opt Laser Technol 103:367–372. https://doi.org/10.1016/j.optlastec.2018.01.057

18. Tahir MB, Nabi G, Iqbal T, Sagir M, Rafique M (2018) Role of $MoSe_2$ on nanostructures WO_3-CNT performance for photocatalytic hydrogen evolution. Ceram Int 44:6686–6690. https://doi.org/10.1016/j.ceramint.2018.01.081

19. Silva MA, Hilliou L, de Amorim MP (2019) Fabrication of pristine-multiwalled carbon nanotubes/cellulose acetate composites for removal of methylene blue. Polym Bull 77:623–653. https://doi.org/10.1007/s00289-019-02769-0

20. Maria KH, Mieno T (2017) Production and properties of carbon nanotube/cellulose composite paper. J Nanomater 2017:1–11. https://doi.org/10.1155/2017/6745029

21. Mougel JB, Bertoncini P, Cathala B, Chauvet O, Capron I (2019) Macroporous hybrid Pickering foams based on carbon

nanotubes and cellulose nanocrystals. J Colloid Interface Sci 544:78–87. https://doi.org/10.1016/j.jcis.2019.01.127

22. Ariyadejwanich P, Tanthapanichakoon W, Nakagawa K, Mukai S, Tamon H (2003) Preparation and characterization of mesoporous activated carbon from waste tires. Carbon 41:157–164. https://doi.org/10.1016/S0008-6223(02)00267-1

23. Machin EB, Pedroso DT, de Carvalho Jr JA (2017) Energetic valorization of waste tires. Renew Sustain Energy Rev 68:306–315. https://doi.org/10.1016/j.rser.2016.09.110

24. Di Leo G, Fisci E, Secchi F, Alì M, Ambrogi F, Sconfienza LM, Sardanelli F (2016) Diagnostic accuracy of magnetic resonance angiography for detection of coronary artery disease: a systematic review and meta-analysis. Eur Radiol 26:3706–3718. https://doi.org/10.1007/s00330-015-4134-0

25. Shi H, Li W, Zhong L, Xu C (2014) Methylene blue adsorption from aqueous solution by magnetic cellulose/graphene oxide composite: equilibrium, kinetics, and thermodynamics. Ind Eng Chem Res 53:1108–1118. https://doi.org/10.1021/ie4027154

26. Liang C, Liu H, Zhou J, Peng X, Zhang H (2015) One-step synthesis of spherical γ-Fe_2O_3 nanopowders and the evaluation of their photocatalytic activity for orange I degradation, Journal of Chemistry, 2015, https://doi.org/10.1155/2015/791829

27. Mwafy EA (2020) Eco-friendly approach for the synthesis of MWCNTs from waste tires via chemical vapor deposition. Environmental Nanotechnology, Monitoring & Management 14:100342. https://doi.org/10.1016/j.enmm.2020.100342

28. Su P-G, Yu J-H, Chen I-C, Syu H-C, Chiu S-W, Chou T-I (2019) Detection of ppb-level NO_2 gas using a portable gas-sensing system with a Fe_2O_3/MWCNTs/WO_3 sensor using a pulsed-UV-LED. Anal Methods 11:973–979. https://doi.org/10.1039/C8AY02500B

29. Cai D, Song M (2007) Water-Based Polyurethane Filled with Multi-Walled Carbon Nanotubes Prepared by a Colloidal-Physics Method Author: This manuscript has been thoroughly edited Please read the proofs carefully to ensure that no unintentional shift in meaning has been introduced. , Macromolecular Chemistry and Physics 208:1183–1189. https://doi.org/10.1002/macp.200600654

30. Yu H, Huang T, Lu M, Mao M, Zhang Q, Wang H (2013) Enhanced power output of an electrospun PVDF/MWCNTs-based nanogenerator by tuning its conductivity. Nanotechnology 24:405401. https://doi.org/10.1088/0957-4484/24/40/405401/meta

31. Luo X, Wang J, Dooner M, Clarke J (2015) Overview of current development in electrical energy storage technologies and the application potential in power system operation. Appl Energy 137:511–536. https://doi.org/10.1016/j.apenergy.2014.09.081

32. Bo S, Luo J, An Q, Xiao Z, Wang H, Cai W, Zhai S, Li Z (2020) Efficiently selective adsorption of Pb (II) with functionalized alginate-based adsorbent in batch/column systems: Mechanism and application simulation. J Clean Prod 250:119585. https://doi.org/10.1016/j.jclepro.2019.119585

33. Jiang D, Yang Y, Huang C, Huang M, Chen J, Rao T, Ran X (2019) Removal of the heavy metal ion nickel (II) via an adsorption method using flower globular magnesium hydroxide. J Hazard Mater 373:131–140. https://doi.org/10.1016/j.jhazmat.2019.01.096

34. Fu J, Chen Z, Wang M, Liu S, Zhang J, Zhang J, Han R, Xu Q (2015) Adsorption of methylene blue by a high-efficiency adsorbent (polydopamine microspheres): kinetics, isotherm, thermodynamics and mechanism analysis. Chem Eng J 259:53–61. https://doi.org/10.1016/j.cej.2014.07.101

35. Kırbıyık C, Pütün AE, Pütün E (2017) Equilibrium, kinetic, and thermodynamic studies of the adsorption of Fe (III) metal ions and 2, 4-dichlorophenoxyacetic acid onto biomass-based activated carbon by $ZnCl_2$ activation. Surfaces and Interfaces 8:182–192. https://doi.org/10.1016/j.surfin.2017.03.011

36. Yahya M, Aliyu A, Obayomi K, Olugbenga A, Abdullahi U (2020) Column adsorption study for the removal of chromium and manganese ions from electroplating wastewater using cashew nutshell adsorbent. Cogent Engineering 7:1748470. https://doi.org/10.1080/23311916.2020.1748470

37. Yahya MD, Odigure J (2015) Fixed bed column study for Pb (II) adsorption using Calcium-Alginate treated shea butter husk (TSBH), 2015 International Conference on Industrial Engineering and Operations Management (IEOM), IEEE, pp. 1–9. https://doi.org/10.1109/IEOM.2015.7093936

38. Egbosiuba TC, Abdulkareem AS, Kovo AS, Afolabi EA, Tijani JO, Bankole MT, Bo S, Roos WD (2021) Adsorption of Cr (VI), Ni (II), Fe (II) and Cd (II) ions by KIAgNPs decorated MWCNTs in a batch and fixed bed process. Sci Rep 11:1–20. https://doi.org/10.1038/s41598-020-79857-z

39. El Badawi N, Ramadan AR, Esawi AM, El-Morsi M (2014) Novel carbon nanotube–cellulose acetate nanocomposite membranes for water filtration applications. Desalination 344:79–85. https://doi.org/10.1016/j.desal.2014.03.005

40. Yu X, Tong S, Ge M, Zuo J, Cao C, Song W (2013) One-step synthesis of magnetic composites of cellulose@ iron oxide nanoparticles for arsenic removal. Journal of Materials Chemistry A 1:959–965. https://doi.org/10.1039/C2TA00315E

41. Egbosiuba T, Abdulkareem A, Kovo A, Afolabi E, Tijani J, Roos W (2020) Enhanced adsorption of As (V) and Mn (VII) from industrial wastewater using multi-walled carbon nanotubes and carboxylated multi-walled carbon nanotubes. Chemosphere 254:126780. https://doi.org/10.1016/j.chemosphere.2020.126780

42. Bhavani P, Reddy NR, Reddy IVS, Sakar M (2017) Manipulation over phase transformation in iron oxide nanoparticles via calcination temperature and their effect on magnetic and dielectric properties. IEEE Trans Magn 53:1–5. https://doi.org/10.1109/TMAG.2017.2715320

43. Zhou S, Wang D, Sun H, Chen J, Wu S, Na P (2014) Synthesis, characterization, and adsorptive properties of magnetic cellulose nanocomposites for arsenic removal. Water Air Soil Pollut 225:1–13. https://doi.org/10.1007/s11270-014-1945-6

44. Ahmadpour N, Sayadi MH, Homaeigohar S (2020) A hierarchical Ca/TiO_2/NH_2-MIL-125 nanocomposite photocatalyst for solar visible light induced photodegradation of organic dye pollutants in water. RSC Adv 10:29808–29820. https://doi.org/10.1039/D0RA05192F

45. Likhitha M, Sailaja R, Priyambika V, Ravibabu M (2014) Microwave assisted synthesis of guar gum grafted sodium acrylate/cloisite superabsorbent nanocomposites: Reaction parameters and swelling characteristics. Int J Biol Macromol 65:500–508. https://doi.org/10.1016/j.ijbiomac.2014.02.008

46. Sharma G, Kumar A, Chauhan C, Okram A, Sharma S, Pathania D, Kalia S (2017) Pectin-crosslinked-guar gum/SPION nanocomposite hydrogel for adsorption of m-cresol and o-chlorophenol. Sustainable Chemistry and Pharmacy 6:96–106. https://doi.org/10.1016/j.scp.2017.10.003

47. Gao G-H, Lei Y-H, Dong L-H, Liu W-C, Wang X-F, Chang X-T, Liu T, Yin Y-S, Ajayan PM (2012) Synthesis of nanocomposites of silver nanoparticles with medical stone and carbon nanotubes for their antibacterial applications. Mater Express 2:85–93. https://doi.org/10.1166/mex.2012.1056

48. Ahmadpour N, Sayadi MH, Sobhani S, Hajiani M (2020) Photocatalytic degradation of model pharmaceutical pollutant by novel magnetic TiO_2@$ZnFe_2O_4$/Pd nanocomposite with enhanced photocatalytic activity and stability under solar light irradiation. J Environ Manag 271:110964. https://doi.org/10.1016/j.jenvman.2020.110964

49. Kumanek B, Stando G, Wróbel P, Krzywiecki M, Janas D (2019) Thermoelectric properties of composite films from multi-walled carbon nanotubes and ethyl cellulose doped with heteroatoms.

Synth Met 257:116190. https://doi.org/10.1016/j.synthmet.2019.116190

50. Yan Y, Tang H, Wu F, Wang R, Pan M (2017) One-step self-assembly synthesis α-Fe_2O_3 with carbon-coated nanoparticles for stabilized and enhanced supercapacitors electrode. Energies 10:1296. https://doi.org/10.3390/en10091296

51. Zhang S, Zhang F, Pan Y, Jin L, Liu B, Mao Y, Huang J (2018) Multiwall-carbon-nanotube/cellulose composite fibers with enhanced mechanical and electrical properties by cellulose grafting. RSC Adv 8:5678–5684. https://doi.org/10.1039/C7RA11304H

52. Thommes M, Kaneko K, Neimark AV, Olivier JP, Rodriguez-Reinoso F, Rouquerol J, Sing KS (2015) Physisorption of gases, with special reference to the evaluation of surface area and pore size distribution (IUPAC Technical Report). Pure Appl Chem 87:1051–1069. https://doi.org/10.1515/pac-2014-1117/html

53. Che BD, Nguyen L-TT, Nguyen BQ, Nguyen HT, Van Le T, Nguyen NH (2014) Effects of carbon nanotube dispersion methods on the radar absorbing properties of MWCNT/epoxy nanocomposites. Macromol Res 22:1221–1228. https://doi.org/10.1007/s13233-014-2169-8

54. You J, Zhao Y, Wang L, Bao W, He Y (2020) Atomic layer deposition of γ-Fe_2O_3 nanoparticles on modified MWCNT for efficient adsorption of Cr (VI) ions from aqueous solution. J Phys Chem Solids 142:109441. https://doi.org/10.1016/j.jpcs.2020.109441

55. Donia A, Atia A, Abouzayed F (2012) Preparation and characterization of nano-magnetic cellulose with fast kinetic properties towards the adsorption of some metal ions. Chem Eng J 191:22–30. https://doi.org/10.1016/j.cej.2011.08.034

56. Zhu P, Liu Y, Fang Z, Kuang Y, Zhang Y, Peng C, Chen G (2019) Flexible and highly sensitive humidity sensor based on cellulose nanofibers and carbon nanotube composite film. Langmuir 35:4834–4842. https://doi.org/10.1021/acs.langmuir.8b04259

57. Sharma G, Kumar A, Naushad M, García-Peñas A, Ala'a H, Ghfar AA, Sharma V, Ahamad T, Stadler FJ (2018) Fabrication and characterization of Gum arabic-cl-poly (acrylamide) nanohydrogel for effective adsorption of crystal violet dye. Carbohyd Polym 202:444–453. https://doi.org/10.1016/j.carbpol.2018.09.004

58. Maleki A, Hamesadeghi U, Daraei H, Hayati B, Najafi F, McKay G, Rezaee R (2017) Amine functionalized multi-walled carbon nanotubes: single and binary systems for high capacity dye removal. Chem Eng J 313:826–835. https://doi.org/10.1016/j.cej.2016.10.058

59. Sayadi MH, Ghollasimood S, Ahmadpour N, Homaeigohar S (2022) Biosynthesis of the ZnO/SnO2 nanoparticles and characterization of their photocatalytic potential for removal of organic water pollutants. J Photochem Photobiol A: Chemistry 425:113662. https://doi.org/10.1016/j.jphotochem.2021.113662

60. Al Lafi AG, Al Abdullah J (2015) Cesium and cobalt adsorption on synthetic nano manganese oxide: a two dimensional infra-red correlation spectroscopic investigation. Journal of Molecular Structure 1093:13–23. https://doi.org/10.1016/j.molstruc.2015.03.027

61. Al-Maliki WAK, Alobaid F, Kez V, Epple B (2016) Modelling and dynamic simulation of a parabolic trough power plant. J Process Control 39:123–138. https://doi.org/10.1016/j.jprocont.2016.01.002

62. Kargar F, Bemani A, Sayadi MH, Ahmadpour N (2021) Synthesis of modified beta bismuth oxide by titanium oxide and highly efficient solar photocatalytic properties on hydroxychloroquine degradation and pathways. J Photochem Photobiol A: Chemistry 419:113453. https://doi.org/10.1016/j.jphotochem.2021.113453

63. Rezaei A, Rezaei MR, Sayadi MH (2021) Enhanced 3, 5-dimethylphenol photodegradation via adsorption-photocatalysis synergy using FSTRG nanohybrid catalyst. J Mol Liq 335:116546. https://doi.org/10.1016/j.molliq.2021.116546

64. Gong J, Liu J, Chen X, Jiang Z, Wen X, Mijowska E, Tang T (2015) Converting real-world mixed waste plastics into porous carbon nanosheets with excellent performance in the adsorption of an organic dye from wastewater. Journal of Materials Chemistry A 3:341–351. https://doi.org/10.1039/c4ta05118a

65. Zhang H, Sun X, Hubbe M, Pal L (2019) Flexible and pressure-responsive sensors from cellulose fibers coated with multiwalled carbon nanotubes. ACS Appl Electron Mater 1:1179–1188. https://doi.org/10.1021/acsaelm.9b00182

66. Zadeh RJ, Sayadi MH, Rezaei MR (2020) Removal of 2, 4-dichlorophenoxyacetic acid from aqueous solutions by modified magnetic nanoparticles with amino functional groups, J Water Environ Nanotechnol 5, 147–156. https://doi.org/10.22090/JWENT.2020.02.005

67. Zheng C, Zheng H, Wang Y, Sun Y, An Y, Liu H, Liu S (2019) Modified magnetic chitosan microparticles as novel superior adsorbents with huge "force field" for capturing food dyes. J Hazard Mater 367:492–503. https://doi.org/10.1016/j.jhazmat.2018.12.120

68. Zhao L-X, Liang J-L, Li N, Xiao H, Chen L-Z, Zhao R-S (2020) Kinetic, thermodynamic and isotherm investigations of Cu^{2+} and Zn^{2+} adsorption on LiAl hydrotalcite-like compound. Sci Total Environ 716:137120. https://doi.org/10.1016/j.scitotenv.2020.137120

69. Mohammadabad MZ, Moeinaddini M, Nowrouzi M, Rafiee R, Abbasi A (2020) Facile and cost-efficient synthesis of highly efficient CO_2 adsorbents: a pathway towards a green environment. J Porous Mater 27:1659–1668. https://doi.org/10.1007/s10934-020-00945-6

70. Nowrouzi M, Younesi H, Bahramifar N (2017) High efficient carbon dioxide capture onto as-synthesized activated carbon by chemical activation of Persian Ironwood biomass and the economic pre-feasibility study for scale-up. J Clean Prod 168:499–509. https://doi.org/10.1016/j.jclepro.2017.09.080

71. Mohanta J, Dey B, Dey S (2020) Sucrose-triggered, self-sustained combustive synthesis of magnetic nickel oxide nanoparticles and efficient removal of malachite green from water. ACS Omega 5:16510–16520. https://doi.org/10.1021/acsomega.0c00999

72. Sarma P, Kumar R, Pakshirajan K (2015) Batch and continuous removal of copper and lead from aqueous solution using cheaply available agricultural waste materials. International J Environ Res 9:635–648

73. Uddin MT, Rukanuzzaman M, Khan MMR, Islam MA (2009) Adsorption of methylene blue from aqueous solution by jackfruit (Artocarpus heteropyllus) leaf powder: a fixed-bed column study. J Environ Manage 90:3443–3450. https://doi.org/10.1016/j.jenvman.2009.05.030

74. Chen S, Yue Q, Gao B, Li Q, Xu X, Fu K (2012) Adsorption of hexavalent chromium from aqueous solution by modified corn stalk: a fixed-bed column study. Biores Technol 113:114–120. https://doi.org/10.1016/j.biortech.2011.11.110

75. Heydartaemeh M (2018) An innovative application of (Ni_XZn_X–X Fe_2O_4) Mineral nanoparticles for adsorption of Malachite green dye from wastewater effluents, Journal of Mining and Environment, 9, 143–152. https://doi.org/10.22044/JME.2017.5858.1397

76. Kiani G, Dostali M, Rostami A, Khataee AR (2011) Adsorption studies on the removal of Malachite Green from aqueous solutions onto halloysite nanotubes. Appl Clay Sci 54:34–39. https://doi.org/10.1016/j.clay.2011.07.008

77. Vergis BR, Krishna RH, Kottam N, Nagabhushana B, Sharath R, Darukaprasad B (2018) Removal of malachite green from aqueous solution by magnetic $CuFe_2O_4$ nano-adsorbent synthesized by one pot solution combustion method. Journal of Nanostructure in Chemistry 8:1–12. https://doi.org/10.1007/s40097-017-0249-y

78. Ullah S, Ur Rahman A, Ullah F, Rashid A, Arshad T, Viglašová E, Galamboš M, Mahmoodi NM, Ullah H (2021) Adsorption of

malachite green dye onto mesoporous natural inorganic clays: Their equilibrium isotherm and kinetics studies. Water 13:965. https://doi.org/10.3390/w13070965

79. Salamat S, Mohammadnia E, Hadavifar M (2021) Kinetics and adsorption investigation of malachite green onto thiolated graphene oxide nanostructures. Journal of Water and Wastewater 31, 1–11. https://doi.org/10.22093/wwj.2020.208052.2951

80. Rouhi M, Lakouraj MM, Tashakkorian H, Hasantabar V (2019) Novel carbon based bioactive nanocomposites of aniline/indole copolymer for removal of cationic dyes from aqueous solution: kinetics and isotherms. New J Chem 43:2400–2410. https://doi.org/10.1039/C8NJ02924E

81. Robati D, Rajabi M, Moradi O, Najafi F, Tyagi I, Agarwal S, Gupta VK (2016) Kinetics and thermodynamics of malachite green dye adsorption from aqueous solutions on graphene oxide and reduced graphene oxide. J Mol Liq 214:259–263. https://doi.org/10.1016/j.molliq.2015.12.073

82. Moradi O, Sharma G (2021) Emerging novel polymeric adsorbents for removing dyes from wastewater: A comprehensive review and comparison with other adsorbents. Environ Res 111534. https://doi.org/10.1016/j.envres.2021.111534

83. Bayramoglu G, Doz T, Ozalp VC, Arica MY (2017) Improvement stability and performance of invertase via immobilization on to silanized and polymer brush grafted magnetic nanoparticles. Food Chem 221:1442–1450. https://doi.org/10.1016/j.foodchem.2016.11.007

84. Sharma G, Kumar A, Ghfar AA, García-Peñas A, Naushad M, Stadler FJ (2022) Fabrication and Characterization of Xanthan Gum-cl-poly (acrylamide-co-alginic acid) Hydrogel for Adsorption of Cadmium Ions from Aqueous Medium. Gels 8:23. https://doi.org/10.3390/gels8010023